doi:10.14311/ppt.2025.1.10
Plasma Physics and Technology **12**(1):10–15, 2025

ONE-DIMENSIONAL FLUID MODELING OF METHANE DISSOCIATION IN DIELECTRIC BARRIER DISCHARGE: IMPACT OF VOLTAGE AND DIELECTRIC CONSTANT

Y. M. A. Nedjar*, M. Mostefaoui, D. Benyoucef

Laboratory of Electrical Engineering and Renewable Energy (LGEER), Faculty of Technology, Hassiba Benbouali University of Chlef, Chlef 02000, Algeria.

* y.nedjar@univ-chlef.dz

Abstract. This paper presents a one-dimensional simulation of the dielectric barrier discharge (DBD) in pure methane under atmospheric pressure. By employing a fluid model integrated with a set of plasma chemistry to analyze discharge behavior, we study different plasma characteristics, including applied voltage, discharge current, electron and ion density, and diverse chemical species density. Additionally, the study investigates the influences of the variation of applied voltage and the insulation layer constant on the characteristics of the DBD reactor and methane conversion. The findings reveal that increasing the applied voltage and dielectric constant influences the discharge behavior, enhancing methane dissociation.

Keywords: Dielectric barrier discharge, fluid model, methane dissociation, plasma.

1. Introduction

Methane is a potent greenhouse gas that significantly contributes to climate change. Its ability to trap heat far exceeds carbon dioxide, making it a particularly active contributor to global warming despite its relatively short atmospheric longevity [1]. In the pursuit of mitigating methane emissions and converting this greenhouse gas into valuable products, non-thermal plasma technologies have emerged as promising solutions [2, 3]. In particular, dielectric barrier discharge (DBD) plasma technology has emerged as an effective approach for converting methane gas into hydrogen [4]. DBD operate by transmitting a high-voltage through two parallel electrodes covered with insulating layer and separated with gas, which allowed to generate a non-thermal plasma in the discharge gap and ionized methane gas that lead to dissociation process and create new hydrocarbons [5]. Dielectric barrier discharge (DBD) has been extensively employed in numerous industrial applications, including ozone generation, excimer lamps, polymer surface modification, and hydrogen production, proving its adaptability and efficacy in various technological processes [6–9]. Previous studies have reported the efficiency of dielectric barrier discharge in generating hydrogen from methane. Debie et al simulate the methane conversion into higher hydrocarbon in DBD by employing one-dimensional fluid model [10], indarto et al provide a kinetic model for methane conversion in a dielectric barrier discharge (DBD), highlighting the intricate interactions between plasma parameters and reaction pathways that influence overall efficiency and product distribution [11]. In addition, DBD reactor can be optimized by adjusting critical parameters to improve its performance and efficiency. The applied voltage, frequency, electrode configuration, reactor geometry, gas flow rate, and gas composition substantially affect plasma properties and reaction kinetics [12, 13]. This work aims to simulate the dielectric barrier discharge (DBD) in methane gas to understand the plasma discharge physics and dynamics better. The simulation enables the investigation of the behavior, chemistry, and physical properties involved in this process. The model includes a range of electron impact processes for methane, such as elastic momentum transfer, excitation, and ionization [14]. The simulation results can be utilized to study numerous parameters, including the electric field strength, voltage and current, electron density profiles, and density number of newly formed species.

2. Numerical model

2.1. Description of model equations

In this study, the fluid model approach follows the same methodology established in our previous work [15].Through the solution of the drift-diffusion equations, the density of electrons and energy can be determined. The governing equations for the electric discharge, utilizing the drift-diffusion approximation, are provided below [16]:

$$\frac{\partial n_e}{\partial t} + \nabla \mathbf{\Gamma}_e = R_e, \tag{1}$$

where n_e denotes the electron density, $\mathbf{\Gamma}_e$ represents the electron flux vector, and R_e is the source term that accounts for the generation of electrons through ionization and their loss via attachment and recombination processes.

$$\Gamma_e = \mu_e n_e = -\mu_e n_e \mathbf{E} - \nabla n_e D_e \tag{2}$$

with μ_e corresponds to electron mobility, D_e to electron diffusion, and $\mathbf{E}$ to the applied electric field. Electron energy is given by:

$$\frac{\partial n_\varepsilon}{\partial t} + \nabla \mathbf{\Gamma}_\varepsilon + \mathbf{E}.\mathbf{\Gamma}_e = R_\varepsilon \tag{3}$$

with

$$\mathbf{\Gamma}_\varepsilon = -\mu_\varepsilon n_\varepsilon \mathbf{E} - \nabla n_\varepsilon D_\varepsilon. \tag{4}$$

With ε represents the electron energy, n_ε denotes the electron energy density, $\mathbf{\Gamma}_\varepsilon$ is the mean electron energy flux, and R_ε accounts for the energy gained or lost through collisions. The terms μ_ε and D_ε correspond to the electron energy mobility and diffusivity, respectively.

The mean electron energy is calculated using the relation:

$$\varepsilon = \frac{n_\varepsilon}{n_e}. \tag{5}$$

The total electron energy loss is obtained by summing the collisional energy losses over all relevant reactions:

$$R_\varepsilon = \sum_{j=1}^{P} x_j k_j N_n n_\varepsilon \Delta\varepsilon_j, \tag{6}$$

where x_j denoting the mole fraction of the target species involved in reaction j, k_j the rate coefficient for reaction j, N_n the total neutral number density, and $\Delta\varepsilon_j$ the energy loss associated with reaction j, the term P represents the cumulative energy loss due to inelastic electron-neutral collisions.

The electric field is calculated using the following equation:

$$\nabla.\varepsilon_0 \cdot \varepsilon_r \nabla V = \rho_s \tag{7}$$

with V denoting the electrostatic potential, ε_r is the relative permittivity, ε_0 represents the vacuum permittivity, and ρ_s is the space charge density.

The space charge density ρ_s is automatically calculated based on the plasma chemistry defined in the model, using the following expression:

$$\rho_s = q\left(\sum_{k=1}^{N} Z_k n_k - n_e\right), \tag{8}$$

where Z_k denotes the charge number of species k, and q is the elementary charge (the absolute value of the electron charge).

The properties of the dielectric are defined by the following relation:

$$\mathbf{D} = \varepsilon_0 \varepsilon_r \mathbf{E}, \tag{9}$$

where $\mathbf{D}$ denotes the electric field displacement.

Surface charge accumulation occurs on the dielectric surfaces adjacent to the discharge gap, and is governed by the following boundary condition:

$$-\mathbf{n} \cdot (\mathbf{D}_1 - \mathbf{D}_2) = \rho_s \tag{10}$$

$$\frac{\mathrm{d}\rho_s}{\mathrm{d}t} = \mathbf{n} \cdot \mathbf{J}_i + \mathbf{n} \cdot \mathbf{J}_e \tag{11}$$

where ρ_s denotes the surface charge density, and $\mathbf{D}_1$ and $\mathbf{D}_2$ represent the electric displacement fields on either side of the dielectric interface. The terms $\mathbf{n} \cdot \mathbf{J}_i$ and $\mathbf{n} \cdot \mathbf{J}_e$ refer to the total ion and electron current densities at the wall, respectively.

2.2. Plasma chemistry

This section of our work comprises a compilation of potential chemical reactions that may occur in methane gas filled within the discharge gap. These reactions include molecular dissociation, ionization, and excitation processes, which contribute to the formation of reactive intermediates and other hydrocarbon species. A detailed overview of these reactions is presented in Tables 1 and 2

N*	Formula	Type	Δε(eV)	Ref
R_1	$e + CH_4 \Rightarrow e + CH_4$	Elastic	0	[14]
R_2	$e + CH_4 \Rightarrow e + CH_4$	Excitation	0.162	[14]
R_3	$e + CH_4 \Rightarrow e + CH_4$	Excitation	0.362	[14]
R_4	$e + CH_4 \Rightarrow e + CH_3 + H$	Excitation	8.8	[14]
R_5	$e + CH_4 \Rightarrow e + CH_2 + H_2$	Excitation	9.4	[14]
R_6	$e + CH_4 \Rightarrow e + CH + H_2 + H$	Excitation	12.5	[14]
R_7	$e + CH_4 \Rightarrow e + C + H_2 + H_2$	Excitation	14	[14]
R_8	$e + CH_4 \Rightarrow 2e + CH_4^+$	Ionization	12.63	[14]
R_9	$e + CH_4 \Rightarrow 2e + H + CH_3^+$	Ionization	14.25	[14]
R_{10}	$e + CH_4 \Rightarrow 2e + H_2 + CH_2^+$	Ionization	15.1	[14]
R_{11}	$e + CH4 \Rightarrow 2e + H + H_2 + CH^+$	Ionization	19.9	[14]
R_{12}	$e + CH_4 \Rightarrow 2e + H_2 + H_2 + C^+$	Ionization	19.6	[14]
R_{13}	$e + CH_4 \Rightarrow 2e + CH_2 + H_2^+$	Ionization	20.1	[14]
R_{14}	$e + CH_4 \Rightarrow 2e + CH_3 + H^+$	Ionization	18	[14]

Table 1. Electron Collisions with Methane.

N°	Reaction	Rate Coefficient A $\left[\mathrm{m^3/s.mol}\right]$	E [J/mol]	n	Ref
R_1	$CH_4 + CH_2 \Rightarrow CH_3 + CH_3$	0.0713×10^{-16}	41988	0	[17]
R_2	$CH_4 + CH \Rightarrow C_2H_4 + H$	153×10^{-16}	–	−0.9	[18]
R_3	$CH_4 + H \Rightarrow CH_3 + H_2$	2.2×10^{-26}	33632	3	[19]
R_4	$CH_3 + CH_3 \Rightarrow C_2H_6$	4.66×10^{-16}	–	−0.37	[17]
R_5	$CH_3 + CH_3 \Rightarrow C_2H_4 + H_2$	170×10^{-16}	133030	–	[18]
R_6	$CH_3 + CH_3 \Rightarrow C_2H_5 + H$	0.5×10^{-16}	56540	–	[17]
R_7	$CH_3 + CH_2 \Rightarrow C_2H_4 + H$	0.7×10^{-16}	–	–	[17]
R_8	$CH_3 + CH \Rightarrow C_2H_3 + H$	0.5×10^{-16}	–	–	[18]
R_9	$CH_3 + C \Rightarrow C_2H_2 + H$	0.83×10^{-16}	–	–	[18]
R_{10}	$CH_3 + H_2 \Rightarrow CH_4 + H$	1.1×10^{-26}	39410	2.74	[18]
R_{11}	$CH_3 + H \Rightarrow CH_2 + H_2$	1×10^{-16}	63190	–	[17]
R_{12}	$CH_2 + CH_2 \Rightarrow C_2H_4$	0.017×10^{-16}	–	–	[20]
R_{13}	$CH_2 + CH_2 \Rightarrow C_2H_2 + H$	1.8×10^{-16}	3326	–	[18]
R_{14}	$CH_2 + CH_2 \Rightarrow C_2H_2 + H_2$	26.3×10^{-16}	50000	–	[18]
R_{15}	$CH_2 + CH_2 \Rightarrow CH_3 + CH$	4×10^{-16}	41572	–	[18]
R_{16}	$CH_2 + CH \Rightarrow C_2H_2 + H$	0.66×10^{-16}	–	–	[21]
R_{17}	$CH_2 + C \Rightarrow C_2H + H$	0.83×10^{-16}	–	–	[21]
R_{18}	$CH_2 + H_2 \Rightarrow CH_3 + H$	0.19×10^{-16}	53212	0.17	[18]
R_{19}	$CH_2 + H \Rightarrow CH + H_2$	2.2×10^{-16}	–	–	[18]
R_{20}	$CH + CH \Rightarrow C_2H_2$	2×10^{-16}	–	–	[17]
R_{21}	$CH + C \Rightarrow C_2 + H$	0.66×10^{-16}	–	–	[18]
R_{22}	$CH + H_2 \Rightarrow CH_2 + H$	5.46×10^{-16}	16155	–	[18]
R_{23}	$CH + H \Rightarrow C + H_2$	1.13×10^{-16}	665	–	[17]
R_{24}	$C + H_2 \Rightarrow CH + H$	6.64×10^{-16}	97278	–	[17]
R_{25}	$CH_4^+ + CH_4 \Rightarrow CH_5^+ + CH_3$	11.5×10^{-16}	–	–	[20]
R_{26}	$CH_4^+ + H_2 \Rightarrow CH_5^+ + H$	1.086×10^{-16}	−300	−0.14	[18]
R_{27}	$CH_4^+ + H \Rightarrow CH_3^+ + H_2$	0.1×10^{-16}	–	–	[18]
R_{28}	$CH_5^+ + CH_2 \Rightarrow CH_3^+ + CH_4$	9.6×10^{-16}	–	–	[18]
R_{29}	$CH_5^+ + CH \Rightarrow CH_2^+ + CH_4$	120×10^{-16}	–	−0.5	[18]

Table 2. Reactions of Methane with Rate Coefficients.

2.3. Model Geometry Description

The simulation was conducted using a one-dimensional (1D) geometry consisting of two parallel plates, each coated with a dielectric material having a relative permittivity of ε_r=10 and a thickness of 1.5 mm. The discharge gap between the plates is 2 mm and is filled with pure methane gas, as illustrated in Figure 1.

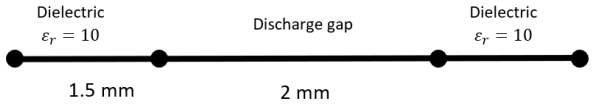

Figure 1. 1D model of DBD reactor with double dielectric barrier.

2.4. Electric potential

An applied voltage of 6 kV powers this model at a high frequency of 3 kHz under atmospheric pressure and a gas temperature of 300 K.

$$V_{\mathrm{rf}} = 6000 \sin(2\pi f) \tag{12}$$

2.5. Initial value

Initial electron and ion density electrons present in the gap:
$\mathbf{n}_{\mathrm{e},0}= 12 \times 10^6\,\mathrm{m}^{-3}$, $\mathbf{n}_{\mathrm{i},0}= 10^6\mathrm{m}^{-3}$
Initial mean electron energy:
ε= 5V

3. Results and discussions

Figure 2, shows the time evolution of applied voltage and current during the discharge across the discharge gap in two period. Notably, two distinct single current events can be observed within each cycle which attributed to breakdown of gas in the gap.

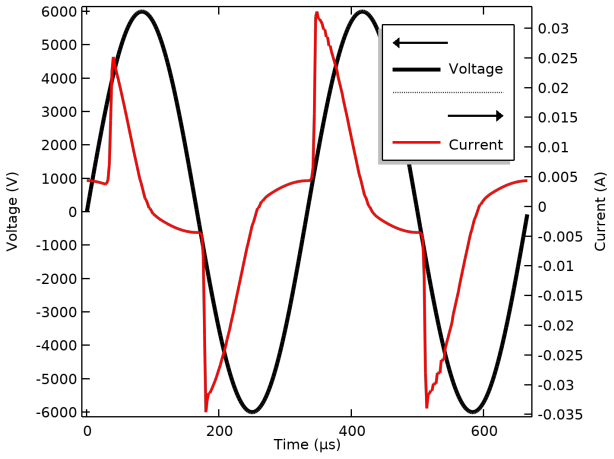

Figure 2. Time evolution of applied voltage and discharge current.

Figure 3 Describes the evolution of the density number for electrons and ions as a function of the distance between electrodes. The electron density decrease gradually from approximately $10^{14}\,\mathrm{m}^{-3}$ near the anode and reducing to $10^6\,\mathrm{m}^{-3}$ as it approaches to the cathode accompanied with increase in ions density, reflecting the ionization processes occurring between electrons and methane molecule within the discharge region, leading to the production of various ionic species according to table 2. Where The most abundant ionic species was CH_4^+, followed by CH_3^+ and CH_2^+.

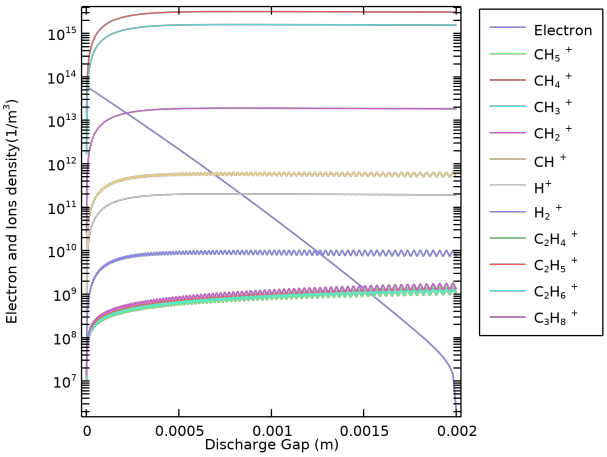

Figure 3. Distribution of electrons, ions across discharge gap and species at t = 400μs.

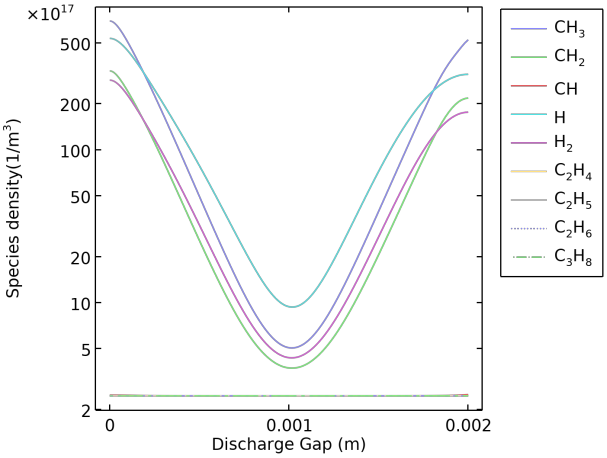

Figure 4. Distribution of species across discharge gap at t = 400μs.

Figure 4 describes the distribution of species across the discharge gap. It can be seen that the species with the highest densities are CH_3, H, CH_2, H_2, particularly near the dielectric boundaries. As species migrate toward the center of the discharge gap, H atoms become the most dominant, in agreement with previous findings [10]. These species are primarily formed via electron-impact reactions with CH_4, as listed in Table 2, as well as through neutral-neutral and ion-neutral reactions, as described in Table 2. However, their densities vary significantly across the discharge region. Near the anode, where the elec-

tric field is strongest, the production rates of radicals are highest due to more energetic electron collisions. As electrons move toward the cathode, their energy decreases, resulting in lower dissociation rates and, consequently, a reduced density of these species. For example, the density of CH_3 near the anode reaches $6.91 \times 10^{19}\,m^{-3}$, compared to $5.32 \times 10^{19}\,m^{-3}$ near the cathode. Similarly, CH_2 and H_2 reach peak values of $3.25 \times 10^{19}\,m^{-3}$ and $2.83 \times 10^{19}\,m^{-3}$, respectively. In contrast, heavier hydrocarbons such as C_2H_2, C_2H_5, C_2H_6, C_3H_8 maintain relatively constant densities throughout the discharge, with typical values around $2.44 \times 10^{17}\,m^{-3}$. This behavior is attributed to a dynamic balance between their formation and consumption rates, as shown in Table 2. The dominance of CH_3, H, CH_2, H_2 as primary products is consistent with general trends observed in low-pressure CCP-RF methane plasmas, where electron-impact dissociation of CH_4 also leads to high concentrations of these species [22, 23].

3.1. Parametric study

Various operational parameters of the discharge system significantly influence the density of hydrogen produced from the DBD reactor. In this section, we study the effect of changing the applied voltage and dielectric constant of insulating on discharge current, density of electrons, and hydrogen.

3.1.1. Influence of applied voltage

In this section, we examine the influence of the applied voltage on the electrical characteristics of a dielectric barrier discharge (DBD) in methane. Specifically, we present the results obtained for three distinct values of the applied voltage: 3 kV, 6 kV, and 9 kV while maintaining a constant frequency of 3 kHz, a gas gap of 2 mm, and employing a dielectric material with a permittivity value of 10.

In Figure 5, we present the effect of variation of applied voltage on discharge current. According to the figure, the discharge current rises as the applied voltage increases, which reaches a value of 0.5 A at 9 kV. Furthermore, we observe a shorter displacement current period at higher applied voltages. This indicates the higher electric field induced by applied voltage, which leads to an increase in ionization rate, which can be seen in figure 6, where electron and ion densities increased as applied voltage rises, where electrons raised from $1 \times 10^{13}\,m^{-3}$ to $2 \times 10^{13}\,m^{-3}$ at 9 kV, CH_4^+ increased from $2.22 \times 10^{12}\,m^{-3}$ to $4.47 \times 10^{12}\,m^{-3}$, and CH_3^+ grew from $1.18 \times 10^{12}\,m^{-3}$ to $2.38 \times 10^{12}\,m^{-3}$. This increased in charged particle density enhances the ionization rate, elevating the discharge current. Additionally, changing the applied voltage also speeds up the dissociation of methane, which increases the density of the species, as is shown in Figure 7, where the density of CH_3 rose from $1.42 \times 10^{19}\,m^{-3}$ to $1.43 \times 10^{20}\,m^{-3}$, that of H rose from $1.13 \times 10^{19}\,m^{-3}$ to $1.11 \times 10^{20}\,m^{-3}$, that of CH_2

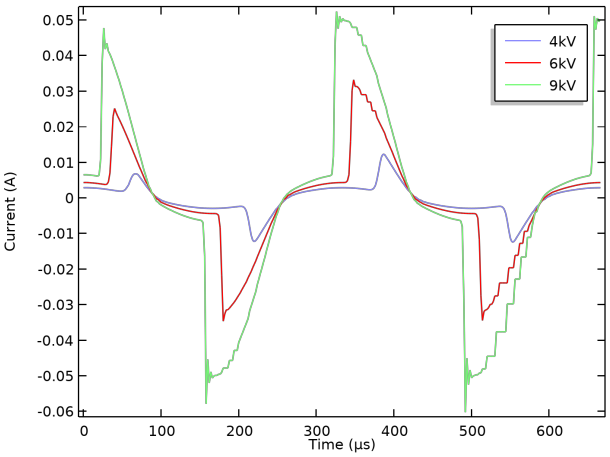

Figure 5. Effect of applied voltage on discharge current.

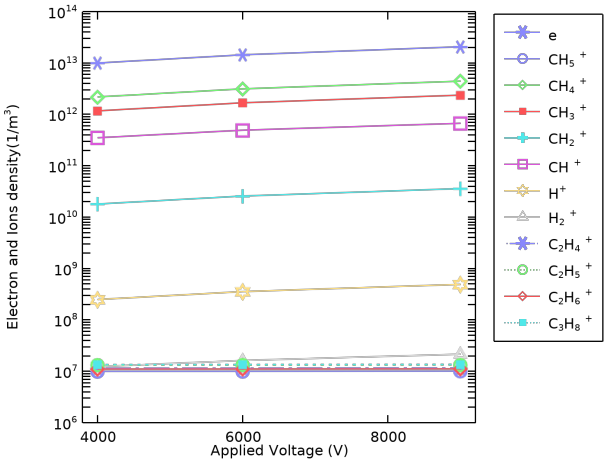

Figure 6. Effect of applied voltage on electron and ion density at $t = 400\mu s$.

rose from $6.78 \times 10^{18}\,m^{-3}$ to $6.78 \times 10^{19}\,m^{-3}$, and that of H_2 rose from $6.04 \times 10^{18}\,m^{-3}$ to $5.92 \times 10^{19}\,m^{-3}$.

3.1.2. Effects of the dielectric constant

The dielectric constant (relative permittivity) of the insulating layer plays a significant role in the performance of dielectric barrier discharge (DBD) reactors. Three representative values of relative permittivity (4.2, 6, and 10) were selected to reflect typical dielectric materials commonly used in DBD systems, such as quartz, borosilicate glass, and zirconia-based ceramics. These values were investigated under fixed conditions of 6 kV applied voltage, 3 kHz frequency, and a 2 mm gas gap to evaluate their influence on discharge characteristics and methane conversion efficiency.

Figure 8 shows the effect of varying the dielectric constant on the discharge current. As the dielectric constant increases, the discharge current correspondingly rises, reaching a peak of 0.03 A at the highest dielectric constant utilized in this study. Additionally, the effect of the dielectric constant on the densities of electrons and ions was examined. The electron density rose from $6.18 \times 10^{12}\,m^{-3}$ to $1.44 \times 10^{13}\,m^{-3}$, while the

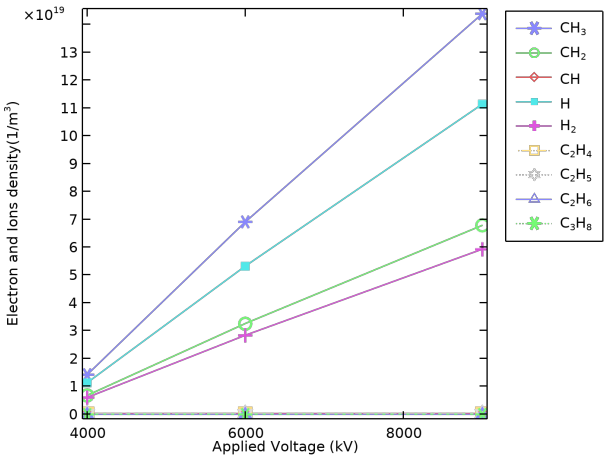

Figure 7. Effect of applied voltage on species density at $t = 400\mu s$.

CH_4^+ grew from $1.34 \times 10^{19}\,m^{-3}$to $3.13 \times 10^{19}\,m^{-3}$, as illustrated in Figure 9. This increase in densities refers to Materials with higher dielectric constants that enhance the capacitance of the dielectric barrier, leading to increased discharge intensity, which strengthens the local electric field and ionization rate.

In Figure 10, we can note an increase in species density of CH_3, which raised from $2.38 \times 10^{19}\,m^{-3}$ to $6.96 \times 10^{19}\,m^{-3}$, H increased from $1.84 \times 10^{19}\,m^{-3}$ to $5.37 \times 10^{19}\,m^{-3}$, CH_2 grows from $1.13 \times 10^{19}\,m^{-3}$ to $3.25 \times 10^{19}\,m^{-3}$, and H_2 raised from $9.8 \times 10^{18}\,m^{-3}$ to $2.86 \times 10^{19}\,m^{-3}$.

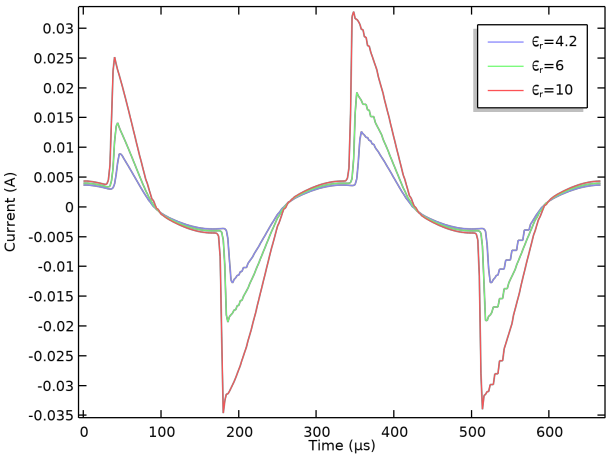

Figure 8. Effect of applied voltage on discharge current.

4. Conclusion

In this study, we developed a one-dimensional fluid model to simulate dielectric barrier discharge (DBD) processes for methane dissociation at atmospheric pressure. The model integrates electrical and chemical modules, enabling the examination of discharge characteristics such as applied voltage and current and kinetic parameters, including the densities of electrons, ions, and various chemical species. By adjusting DBD

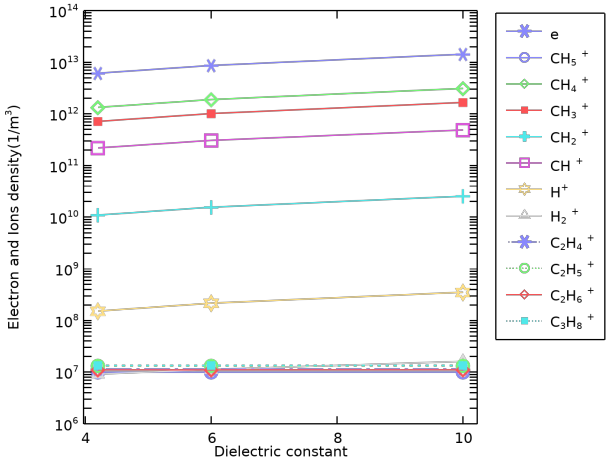

Figure 9. Effect of dielectric constant on electron and ion density at $t = 400\mu s$.

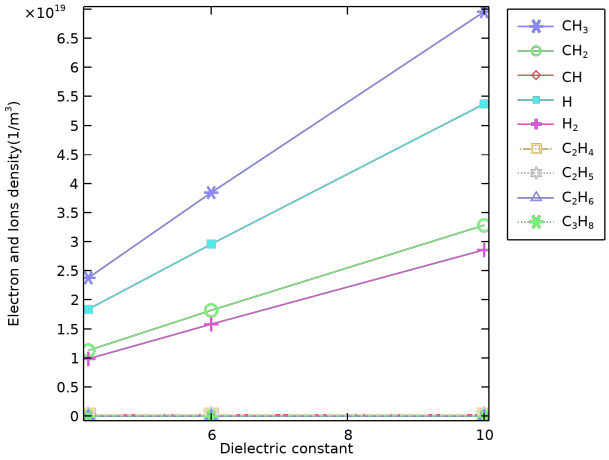

Figure 10. Effect of dielectric constant on on species density at $t = 400\mu s$.

actuator parameters, we aimed to optimize methane dissociation efficiency, which is vital for applications of reducing greenhouse gas emissions. One of the important results was the growing density of hydrogen, which is used in fuel cells. Our findings indicate that increasing the applied voltage and dielectric constant significantly enhances the ionization rate of methane gas. However, the presence of other hydrocarbons affects the efficiency of the DBD reactor, which can alter the distribution of reactive species, potentially leading to reduced selectivity for desired products such as hydrogen. Therefore, further studies are necessary to optimize methane dissociation into valuable products like hydrogen. Future research should explore the effects of different gas compositions, reactor configurations, and operating conditions to enhance selectivity and yield.

References

[1] The national aeronautics and space administration. https://climate.nasa.gov/vital-signs/methane/?intent=121 [Accessed: (15-12-2024)].

[2] S. Meng, W. Li, Z. Li, and H. Song. Non-thermal

plasma assisted non-oxidative methane liquefaction for fuel production at near ambient conditions. *Catal. Sci. Technol.*, 13:4665–4672, 2023. doi:10.1039/D3CY00835E.

[3] R. S. Abiev, D. A. Sladkovskiy, K. V. Semikin, et al. Non-thermal plasma for process and energy intensification in dry reforming of methane. *Catalysts*, 10(11), 2020. doi:10.3390/catal10111358.

[4] Z. Zhou, J. Zhang, T. Ye, et al. Hydrogen production by reforming methane in a corona inducing dielectric barrier discharge and catalyst hybrid reactor. *Chinese Science Bulletin*, 56(20):2162–2166, July 2011. doi:10.1007/s11434-011-4485-0.

[5] U. Kogelschatz. Dielectric-Barrier Discharges: Their History, Discharge Physics, and Industrial Applications. *Plasma Chemistry and Plasma Processing*, 23(1):1–46, 2003. doi:10.1023/A:1022470901385.

[6] X. Gou, D. Yuan, L. Wang, et al. Enhancing ozone production in dielectric barrier discharge utilizing water as electrode. *Vacuum*, 212:112047, 2023. doi:10.1016/j.vacuum.2023.112047.

[7] H. Loukil, N. Larbi Daho Bachir, K. Khodja, et al. Experimental study of optical emission in the dbd excimer lamp containing a mixture of neon xenon. *Optik*, 269:169910, 2022. doi:10.1016/j.ijleo.2022.169910.

[8] G. Borcia, C. A. Anderson, and N. M. D. Brown. Dielectric barrier discharge for surface treatment: application to selected polymers in film and fibre form. *Plasma Sources Science and Technology*, 12(3):335, may 2003. doi:10.1088/0963-0252/12/3/306.

[9] S. S. Kim, M. Jorat, G. Voecks, et al. Hydrogen from steam methane reforming by catalytic nonthermal plasma using a dielectric barrier discharge reactor. *AIChE Journal*, 66(4):e16880, 2020.

[10] C. De Bie, B. Verheyde, T. Martens, et al. Fluid Modeling of the Conversion of Methane into Higher Hydrocarbons in an Atmospheric Pressure Dielectric Barrier Discharge. *Plasma Processes and Polymers*, 8(11):1033–1058, November 2011. doi:10.1002/ppap.201100027.

[11] A. Indarto, N. Coowanitwong, J.-W. Choi, et al. Kinetic modeling of plasma methane conversion in a dielectric barrier discharge. *Fuel Processing Technology*, 89(2):214–219, 2008. doi:10.1016/j.fuproc.2007.09.006.

[12] B. Wang, X. Zhang, H. Bai, et al. Hydrogen production from methanol through dielectric barrier discharge. *Frontiers of Chemical Science and Engineering*, 5(2):209–214, June 2011. doi:10.1007/s11705-010-1018-3.

[13] P.-A. Maitre, J. Long, M. S. Bieniek, et al. Investigating the effects of helium, argon and hydrogen co-feeding on the non-oxidative coupling of methane in a dielectric barrier discharge reactor. *Chemical Engineering Science*, 259:117731, 2022. doi:10.1016/j.ces.2022.117731.

[14] A. Gadoum and D. Benyoucef. Set of the electron collision cross sections for methane molecule. *IEEE Transactions on Plasma Science*, 47(3):1505–1513, 2019. doi:10.1109/TPS.2018.2885610.

[15] N. Yahia Mohamed Amine, M. Mohamed, and B. Djilali. Investigation of ar/ch_4 mixtures in dielectric barrier discharge: A simulation approach for hydrogen production. *Bulletin of Chemical Reaction Engineering & Catalysis*, 20(3):458–470, October 2025. doi:10.9767/bcrec.20352.

[16] G. J. M. Hagelaar and L. C. Pitchford. Solving the Boltzmann equation to obtain electron transport coefficients and rate coefficients for fluid models. *Plasma Sources Science and Technology*, 14(4):722–733, November 2005. doi:10.1088/0963-0252/14/4/011.

[17] Nist chemical kinetics database. http://kinetics.nist.gov/kinetics/ [Accessed: (05-05-2024)].

[18] The umist database for astrochemistry. http://udfa.ajmarkwick.net/index.php [Accessed: (05-05-2024)].

[19] The kinetic database for astrochemistry. https://kida.astrochem-tools.org/ [Accessed: (05-05-2024)].

[20] W. Huntress. Laboratory studies of bimolecular reactions of positive ions in interstellar clouds, in comets, and in planetary atmospheres of reducing composition. *The Astrophysical Journal Supplement Series*, 33:495, 04 1977. doi:10.1086/190439.

[21] M. Mao and A. Bogaerts. Investigating the plasma chemistry for the synthesis of carbon nanotubes/nanofibres in an inductively coupled plasma enhanced cvd system: the effect of different gas mixtures. *Journal of Physics D: Applied Physics*, 43(20):205201, may 2010. doi:10.1088/0022-3727/43/20/205201.

[22] C.-W. Chang, M. Davoudabadi, and F. Mashayek. One-dimensional fluid model of methane plasma for diamond-like coating. *IEEE Transactions on Plasma Science*, 38(7):1603–1614, 2010. doi:10.1109/TPS.2010.2049750.

[23] D. Herrebout, A. Bogaerts, M. Yan, et al. One-dimensional fluid model for an rf methane plasma of interest in deposition of diamond-like carbon layers. *Journal of Applied Physics*, 90(2):570–579, July 2001. doi:10.1063/1.1378059.